Huybrechts, Nicolas; Tassi, Pablo; Villaret, Catherine

Application of TELEMAC-3D to sediment-laden flow on flat bed configuration

Application of TELEMAC-3D to sediment-laden flow on flat bed configuration

Nicolas Huybrechts
Roberval Laboratory, LHN (joint research unit UTC-CETMEF), UMR CNRS 7337
Compiègne, France
nicolas.huybrechts@developpement-durable.gouv.fr

Pablo Tassi and Catherine Villaret
EDF R&D – LNHE – LHSV
Chatou, France
pablo.tassi@edf.fr
catherine.villaret}@edf.fr

***Abstract*—The development of three-dimensional (3D) sediment transport model remains a challenging task, due to our limited knowledge of the complex sediment turbulent flow interactions, as well as the inherent difficulty to represent numerically the large gradients of flow and sediment distribution. In this work, we compare 3D numerical simulations of coupled flow and suspended sediment transport with some well documented flume data. In order to isolate the effect of particles in suspension on the turbulent flow field, we mimic starved bed experiments, where sediment is progressively added to the clear flow below saturation (no deposit). Numerical simulations are based on the TELEMAC-3D module of the open-source TELEMAC Modelling System release 6.2.**

I. INTRODUCTION

Despite some recent progress, the development of full three-dimensional (3D) sediment transport models remains a challenging task [1,2,3]. In addition to our limited knowledge of complex processes which govern sediment/turbulent flow interactions, the inherent difficulty to capture both flow and sediment concentration vertical structures has not been emphasised enough. Other issues such as the influence of suspended sediment on the damping of turbulence level are still subject to continual development and discussion.

The effect of sediment particles and turbulent flow interactions is an intriguing and difficult problem: the inhomogeneous and anisotropic characteristics of a turbulent flow, added to the broad range of involved length and time scales [4], make the problem challenging from both theoretical and computational point of view. In the high concentrated bed-load layer, the effect of particle/particle interaction plays a dominant role and a complete two-phase flow approach is required to capture entirely the near-bed processes [4,5]. In the upper part of the flow, in the dilute suspension regime, particles in suspension can be treated as a passive scalar which interacts with the turbulent flow through density gradients [6].

Turbulence models play a crucial role for predicting both velocity and sediment distribution in the water column, and therefore to estimate accurately the suspended sediment transport rate. The simplest turbulence models assume the turbulent eddy viscosity to be either constant over the flow region, or proportional to the velocity or length scales. The value of the eddy-viscosity is therefore determined entirely by the local flow conditions. The widely used k-ε turbulence model solves two additional transport equations to determine both turbulent kinetic energy k and the rate of dissipation rate ε. The k-equation can be derived in its exact form from the Navier-Stokes equations, while in the ε-equation, all terms are modeled and introduced as a set of semi-empirical 'invariant' model coefficients [7]. In k-ε turbulence models, the sediment induced stratification effect is accounted for, in a straight-forward manner, by the buoyancy term. In eddy viscosity models, the effect of sediment concentration on the turbulence can be represented by using damping functions. These semi-empirical functions are in general expressed as a function of the flux Richardson number, which is defined as the ratio between the gravity term versus the production term in the k-equation.

The objective of this paper is to propose a database for validation of the hydrodynamic module TELEMAC-3D and its sediment transport library Sedi-3D based on the numerical reproduction of the experimental tests by Lyn [4, 8]. In order to isolate the effect of particles in suspension on the turbulent flow field, we mimic the starved bed experiments, where sediment is progressively added to the clear flow below saturation (no deposit). We discuss the sensitivity of the model results to the choice of turbulence closure, friction equation and damping functions, in order to provide practical recommendations for modelling three-dimensional flows and suspended transport. For this work, the numerical simulations are based on the open-source TELEMAC Modelling System release 6.2.

This paper is organised as follows. In Part II, we present the hydrodynamics and sediment transport equations, as well as the different turbulence closure relationships which are implemented in TELEMAC-3D. In Part III, we give a short

literature review on the problem of turbulent flow interactions with suspended sediments. In Part IV, we present the experimental setup used by Lyn [4, 8]. In Part V, we present the discretization of the domain as well as a brief description of the boundary conditions implemented in the flow and sediment transport models. In Part VI, the comparison between data and numerical results is presented and discussed for the clear water and starved bed conditions. Finally, the conclusions and practical recommendations for the TELEMAC-3D end-user are given in Part VII.

II. 3D MATHEMATICAL MODEL OF SUSPENDED SEDIMENT TRANSPORT

A. 3D flow model

The 3D flow field is determined by solving the continuity and Reynolds-averaged Navier-Stokes equations (RANS) in the Cartesian coordinate system:

$$\begin{cases} \dfrac{\partial u_i}{\partial x_i} = 0 \\ \dfrac{\partial u_i}{\partial t} + \dfrac{\partial u_i u_j}{\partial x_j} = F_i - \dfrac{1}{\rho}\dfrac{\partial p}{\partial x_i} + \dfrac{1}{\rho}\dfrac{\partial \tau_{ij}}{\partial x_j}, \end{cases} \quad (1)$$

where the summation convention for repeated indices is used. Above, let $x_i=(x_1,x_2,x_3)=(x,y,z)$ denote the spatial coordinates; $t \geq 0$ the time; $u_i=(u_1,u_2,u_3)=(u,v,w)$ the mean flow velocity, F_i the components of external forces, such as gravity, Coriolis force, etc.; p the mean pressure; ρ the fluid density; and τ_{ij} the components of the stress tensor calculated with the Boussinesq hypothesis and related to the gradients of the velocity and the turbulence eddy viscosity ν_t :

$$-\frac{1}{\rho}\frac{\partial \tau_{ij}}{\partial x_j} = \frac{\partial}{\partial x_j}\left[(\nu + \nu_t)\left(\frac{\partial u_i}{\partial x_j} + \frac{\partial u_j}{\partial x_i} \right) - \frac{2}{3} k \delta_{ij} \right] \quad (2)$$

Above, ν is the kinematic viscosity, k is the turbulent kinetic energy and δ_{ij} is the Kroneker delta.

B. Turbulence closure

In TELEMAC-3D, the eddy viscosity ν_t is determined by the choice of the turbulence closure models. In this paper, we will compare two models: the mixing-length model [9] and the standard k-ε model [7].

In mixing length models, the eddy viscosity model is calculated as a function of mean flow velocity gradients and mixing length l_m:

$$\nu_t = l_m^{\,2} \sqrt{\left(\frac{\partial U}{\partial z}\right)^2 + \left(\frac{\partial V}{\partial z}\right)^2} \quad (3)$$

Following [9], the mixing length is assumed to vary with distance from the bed z,

$$l_m = \kappa z \sqrt{(1 - z/h)} \quad (4)$$

where z =0 is the bed level, h the local water-depth and κ = 0.4 the Karman constant.

In k-ε turbulence models, the eddy viscosity ν_t is related to the turbulent kinetic energy k and the rate of dissipation ε :

$$\nu_t = c_\mu \frac{k^2}{\varepsilon} \quad (5)$$

with c_μ a constant. The governing equations for k and ε are given by:

$$\frac{\partial k}{\partial t} + u_j \frac{\partial k}{\partial x_j} = \frac{\partial}{\partial x_j}\left(\frac{\nu_t}{\sigma_k} \frac{\partial k}{\partial x_j} \right) + P + G - \varepsilon \quad (6)$$

$$\frac{\partial \varepsilon}{\partial t} + u_j \frac{\partial \varepsilon}{\partial x_j} = \frac{\partial}{\partial x_j}\left(\frac{\nu_t}{\sigma_\varepsilon} \frac{\partial \varepsilon}{\partial x_j} \right) + c_1 \frac{\varepsilon}{k} P + c_3 \frac{\varepsilon}{k} G - c_2 \frac{\varepsilon^2}{k} \quad (7)$$

Above c_1, c_2, c_3, σ_k and σ_e are constants. P is the shear production and G the buoyancy term due to density effects (as discussed in Part III), defined as :

$$P = -\overline{u_i' u_j'} \frac{\partial u_i}{\partial x_j} \quad (8)$$

$$G = -g \frac{\overline{\rho' w'}}{\rho} \quad (9)$$

with g the gravity acceleration ($g=9.81 m^2/s$), and $-\overline{u_i' u_i'}$ the turbulent Reynolds stress components. The mean (time or spatially) averaged and fluctuating components of instantaneous quantity x are designated by $\bar{x}$ and x', respectively.

The standard coefficients of the turbulence k-ε model [7] are implemented and can be modified (see for example subroutine CSTKEP):

$c_\mu = 0.09$, $c_1 = 1.44$, $c_2 = 1.92$
$\sigma_k = 1.0$, $\sigma_\varepsilon = 1.3$

C. Sediment transport model

Assuming sediment particles follow the mean and turbulent flow component, except for an additional settling term, the following 3D transport/diffusion equation can be derived:

$$\frac{\partial c}{\partial t} + \frac{\partial u_j c}{\partial x_j} - w_s \frac{\partial c}{\partial x_3} = \frac{\partial}{\partial x_j}\left(\varepsilon_s \frac{\partial c}{\partial x_j} \right) \quad (10)$$

with $c = c(x_i, t)$ the suspended sediment mean (volume) concentration, $w_s > 0$ the vertical-settling sediment velocity and ε_s the turbulent eddy diffusivity coefficient.

The turbulent eddy diffusivity coefficient is assumed to be proportional to the turbulent eddy viscosity: $\varepsilon_s = \nu_t / \sigma_s$, where σ_s is the turbulent Schmidt number.

The advection-diffusion equation (10) is completed with initial and boundary conditions. In this work (starved bed experiments), we assume zero flux at the free surface (z=h), and at the bed: $-\varepsilon_s \, \partial c/\partial z - w_s = 0$. Further details on the implementation of the boundary conditions are given in Part V.

III. SEDIMENT-TURBULENT FLOW INTERACTIONS

A. Sediment induced density gradients

Assuming dilute suspension, such that particle interactions can be neglected, the effect of sediment particles is to increase the density of the flow-sediment mixture:

$$\rho = \rho_s c + \rho_0 (1 - c) \tag{11}$$

where ρ_s is the solid density (assumed ρ_s=2650 kg/m^3), c the volume concentration and ρ_0, the fluid density. The density variation is calculated (subroutine DSRUR) :

$$\frac{\Delta\rho}{\rho_0} = \frac{(\rho_s - \rho_0)}{\rho_0} \frac{C_s}{\rho_s} \tag{12}$$

where $\Delta\rho = \rho - \rho_0$, and $C_s = \rho_s c$ is the mass concentration.

Since most particles are carried near the bed ($\partial\rho/\partial z$ <0), the effect of stable density gradients is to extract turbulent kinetic energy. Indeed the gravity term G in the turbulent kinetic energy equation (7) is a dissipative term:

$$G = \frac{g}{\rho_0} \frac{\nu_t}{\sigma_s} \frac{\partial\rho}{\partial z} < 0 \tag{13}$$

The damping of turbulence can be expressed in terms of the flux Richardson number R_i which is defined as the ratio of the gravity term and the production term in Eqs (8, 9).

$$Ri = -\frac{G}{P} = -\frac{g}{\rho_0} \frac{1}{\sigma_s} \frac{\dfrac{\partial\rho}{\partial z}}{\left(\dfrac{\partial u}{\partial z}\right)^2 + \left(\dfrac{\partial v}{\partial z}\right)^2} \tag{14}$$

B. Damping functions

The effect of particles is analogous to the effect of thermal stratification, and can be represented in eddy viscosity models by use of damping functions [10].

Damping functions are semi-empirical functions that characterise the degree of stratification for both eddy viscosity and eddy diffusivity. They can be expressed as a function of the flux Richardson number R_i, as follows:

$$F_t = (1 + AR_i)^{-a} = \frac{\nu_t}{\nu_0}, \quad F_s = (1 + BR_i)^{-b} = \frac{\varepsilon_s}{\varepsilon_0} \tag{15}$$

with ν_0 and ε_0 the eddy viscosity and sediment diffusion coefficient in neutral conditions respectively, and A, B, a and b a set of empirical coefficients. Different values have been proposed in the literature, as synthesised in Table I.

TABLE I. EXAMPLES OF DAMPING FUNCTION

Damping function	Coefficients			
	A	***a***	***B***	***b***
Munk and Anderson 1948 [10	10	0.5	10/3	1.5
Kranenburg 1998 [11]	2.4	2	2.4	4

According to Villaret and Trowbridge [6], the effect of particles induced stratification effect can be represented by the Munk and Anderson damping function.

C. Effect of particles on the Schmidt number

The value of the Schmidt number for sediment may differ from the classical value used for thermocline (in TELEMAC-3D, this value can be implemented in the subroutine CSTKEP, the default value is σ_s=1.0). For the turbulent Schmidt number (the neutral value), predictive equations were introduced by Graf and Cellino [12] and van Rijn [13]. These equations involve the ratio $ws/u*$, with u_* the friction velocity. For instance, the van Rijn equation [13] is:

$$\frac{1}{\sigma_S} = 1 + 2\left(\frac{W_S}{u_*}\right) \tag{16}$$

Other equations rather link the turbulent Schmidt number to the Richardson number [14].

D. Effect of sediment particles on the apparent bed roughness

The effect of particles in the high concentrated near bed region is to increase the apparent bed roughness [4, 5]. Various semi-empirical formulae have been proposed in the literature in order to account for this process, refer [15, 16] for example.

IV. EXPERIMENTAL DATA

Detailed velocity and concentration profiles have been measured by Lyn [4, 8] using LDV and sediment sampling techniques (or turbidity meter). He conducted flume experiments combining 4 runs with clear water, 7 runs under capacity condition (starved bed) and 4 runs at capacity conditions. This high quality data set will be used here as a new test case for the TELEMAC-3D sediment transport model.

As a first step, we mimic the starved bed experiments, where the concentration is increased progressively in order to isolate the effect of sediment in suspension on the turbulent flow field. The equilibrium data set will be used next to validate the sediment transport model boundary condition.

The flume dimensions are 13 m long and 0.2667 m wide. Velocity and concentration profiles were measured at 9 m from the channel inlet. The main characteristics of each experiment are summarised in Table II. The sediment is a fairly uniform sand of mean diameter d_{50}=0.19 mm and measured settling velocity is approximately w_s=0.023m/s.

TABLE II. SUMMARY OF FLOW AND SEDIMENT PARAMETERS

Runs	Q (l/s)	h (cm)	S (*0.001)	C at 0.1*h (*0.001)	u* (cm/s)
C1	10.84	6.54	2.06	-	3.11
C2	12.66	6.53	2.70	-	3.73
C3	10.77	5.75	2.96	-	3.61
C4	12.66	5.69	4.01	-	4.33
ST1A	10.30	5.69	2.99	0.55	3.74
ST1B	10.30	5.68	2.98	0.24	3.69
ST2A	12.10	5.84	4.00	2.08	4.25
ST2B	12.40	5.77	3.95	0.80	4.31
ST2C	12.60	5.75	4.00	0.47	4.28
ST2D	12.60	4.74	4.00	0.31	4.34

where Q is the flow rate, h the water depth, S the bottom slope and C the concentration level at 10% of the water depth. The friction velocity u* has been computed from the Reynolds stresses measurements [4, 8].

For this work, we have selected the runs C4, ST2B, ST2A as they present relatively similar hydraulic conditions (flow rate, water depth, bed slope) and the highest concentration levels (for the starved bed runs).

V. NUMERICAL SIMULATION

A. Mesh description

The 3D finite element mesh is obtained by first dividing the two-dimensional domain in non-overlapping linear triangles and then by extruding each triangle along the vertical direction into linear prismatic columns that fix the bottom and the free surface and partitioned into a number of non-overlapping layers. In this work, the computational domain is discretised with an unstructured triangular mesh consisting of 2611 nodes, 4682 elements and 12 horizontal layers with vertical grid size increasing with the distance from the bed, in order to represent the large variations of both velocity and concentration profiles. The triangular elements are about 0.85 m size and the first grid plane is located at z/h=0.0178 from the bed level.

B. Hydrodynamic boundary conditions

At the inflow boundary, all flow components are prescribed by imposing a constant flow rate, corresponding to the measurements. The upstream boundary is *indeed* located sufficiently far upstream that is beyond the influence of the channel inflow. Numerical tests with a fully-developed velocity profile calculated from the experimental data showed little variation on the results.

At outlet boundaries, the normal gradients of the flow velocity and sediment concentrations are set equal to zero, whereas the water depth is imposed, according to the experimental measurements. At the sidewalls, the velocities tangential and normal to the boundary are set to zero (no-slip condition).

C. Boundary condition for sediment transport

Boundary conditions for Equation (10) are prescribed as follows. At the inflow boundary, the sediment is assumed to enter the three-dimensional domain with constant concentration. Numerical tests with a local equilibrium concentration profile, calculated from the experimental data, have shown little variation on the results. At outlet boundaries, the normal gradient of sediment concentration is set equal to zero. At the bottom boundary, the vertical fluxes of sediment (both erosion and deposition rates) are set equal to zero. This condition is implemented to mimic the starved-bed flow condition, that assumes that the sand-bed is not present and simplifies the analysis of results [4]. Numerical simulations for the equilibrium bed condition are subject of future work.

D. Friction equation

The Nikuradse friction law is applied, where the velocity at the first elevation plane is related to the friction velocity assuming a classical logarithmic velocity profile:

$$u(z_1) = \frac{u_*}{\kappa} \log\left(\frac{z_1}{z_0}\right) \tag{17}$$

where z_1 is the vertical distance to the first e levation plane from the bed level, u_* is the shear velocity, related to the bed shear stress by $u_* = \sqrt{\tau_b / \rho}$, κ is the von Karman constant (≈ 0.40), $z_0=k_s/30$ is a length scale related to the bottom roughness and k_s the Nikuradse equivalent bed roughness.

E. Turbulence model

For the two-equation turbulence model *k-ε*, the boundary conditions are specified according to Burchard [17]. At the bed level (*z*=0), the boundary condition for the turbulent kinetic energy is given by:

$$k = \frac{u_*^2}{\sqrt{C\mu}} \tag{18}$$

The dissipation decays rapidly with distance from the bed, so it is assumed that $\varepsilon = u_*^3 / \kappa\delta$, where $\delta = z_0$.

At the free surface (*z*=h) and in the absence of wind stress, *k* decreases to zero, we assume $\partial k / \partial z = 0$ whereas ε is reduced to $\varepsilon = k^{3/2} / 0.43h$.

At the channel inlet, the *k-ε* profiles are imposed. Assuming production to balance dissipation, the following analytical expression can be derived [17]:

$$k(z) = \frac{u_*^2 (1 - z/h)}{\sqrt{C_\mu}} \tag{19}$$

$$\varepsilon(z) = \frac{u_*^3 (1 - z/h)}{\kappa z} \tag{20}$$

VI. NUMERICAL RESULTS

A. Results for clear water run C4

For the clear water run, computations have been performed with the mixing length model ('NML', [9]) and the *k-ε* model. For both computations, the roughness height is assumed to be equal to 0.05 mm. The selected value is obtained from a trial and error procedure. The comparison between measured and computed profiles is illustrated in Fig.. 1, where the velocities are normalised by the shear velocity. For this case, the main measured and computed hydrodynamic variables are summarised in Table III.

TABLE III. MAIN HYDRODYNAMIC FEATURES OF RUN C4

C4	data	NML simulation	k- ε simulation
U (m/s)	0.87	0.9	0.9
H (m)	0.0569	0.0557	0.0554
u* (m/s)	0.043	0.038	0.036

Water depth, depth averaged velocity, and shear velocity have mostly the same values for both turbulence models. The computed shear velocity is under-estimated compared to the measured data.

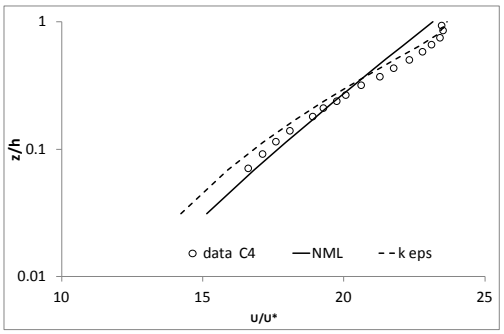

Figure 1. Comparison avec NLM and k- ε models for clear water run C4.

As expected, the computed profile with the NLM model is logarithmic up to the free surface. Below *z/h* = 0.25, the velocity profile is well captured by the NLM model. For *z/h* > 0.25, the measurements do not follow the logarithmic velocity profile. This is probably due to the presence of secondary currents and free surface effects which are not captured in the simple eddy viscosity model: in the upper part of the flow, computed results do not reproduce the observed deviation from the log profile. The velocity profile is overall well captured by the *k-ε* model even if the depth-averaged velocity seems slightly under-predicted.

B. Velocity profiles for sediment-laden flows

The comparison between the NML and the *k-ε* models is performed on the starved bed data sets ST2B and ST2A. These runs are characterised by the highest concentration levels up to 0.64 g/l and 1.46 g/l near the bed (*z/h* = 0.1), respectively. NML simulations are run with and without damping function. To analyse the effect of sediment on the velocity profile for the *k-ε* model, simulations are conducted with and without sediment. The equivalent bed roughness is set equal to 0.7 mm and 1.25 mm for ST2B and ST2A respectively. The velocity profiles for runs ST2B and ST2A are plotted in Fig. 2. The main measured and computed hydrodynamic features are provided in Tables IV and V. The computed water depth, depth averaged velocity and shear velocity are relatively close to the measurements (Tables IV and V).

TABLE IV. MAIN HYDRODYNAMIC FEATURES OF RUN ST2B

ST2B	data	NML simulation	k- ε simulation
U (m/s)	0.862	0.865	0.87
H (m)	0.0577	0.0582	0.0576
u* (m/s)	0.043	0.053	0.047

For run ST2B, even if the concentration level is relatively high, both turbulence models produce almost the same velocity profiles with or without the sediment influence (Fig.

2a). For Run ST2A, *k-ε* model still predicts unchanged velocity profile with or without sediment (Fig. 2c) whereas the velocity profile is influenced by the damping functions with NLM model. For both runs, the detail of the velocity profile is better reproduced by the *k-ε* model. The profiles of the Richardson number (equation (14)) for run ST2B and ST2A are plotted in Fig. 3. The Richardson number reaches high value up to 0.1 near the bed for run ST2A and up to 0.05 for Run ST2B. However, R_i decreases rapidly with distance from the bed, down to less than 1% at about 10% of the water depth which could explain why the *k-ε* model seems not affected by the presence of sediment.

TABLE V. MAIN HYDRODYNAMIC FEATURES OF RUN ST2A

ST2A	data	NML simulation	k- ε simulation
U (m/s)	0.81	0.83	0.83
H (m)	0.0584	0.0583	0.0583
u* (m/s)	0.043	0.046	0.048

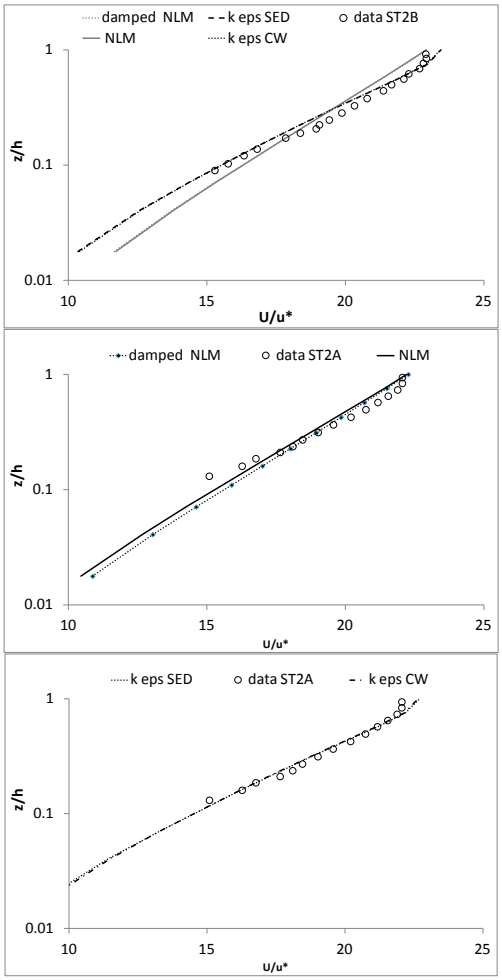

Figure 2. Figure 2. Comparison of NML and k-□ models for runs ST2B and ST2A: (a) velocity profiles for ST2B run; (b) velocity profiles with NML for ST2A run; (c) velocity profiles with k-□ for ST2A run

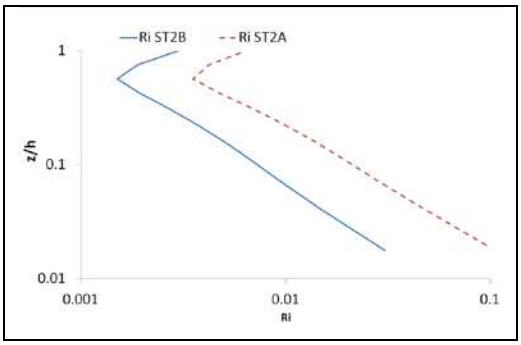

Figure 3. Richardson profiles for run ST2B and ST2A obtained with k-ε model.

C. *Concentration profiles for runs ST2B and ST2A*

For the sediment concentrations, profiles are plotted in Figs. 4a and 4b for runs ST2B and ST2A respectively. The concentration levels are normalised by near bed concentration C_a measured at 10% of the water depth. Results for the concentrations are only shown for the *k-ε* model because the velocity profile is better captured with this turbulence closure. Computations were performed with different values of the turbulent Schmidt number. Best agreements are obtained with σ_s =1.3 or 1.4 for runs ST2B and ST2A respectively. For both runs, the computed concentration profiles match well the experimental data.

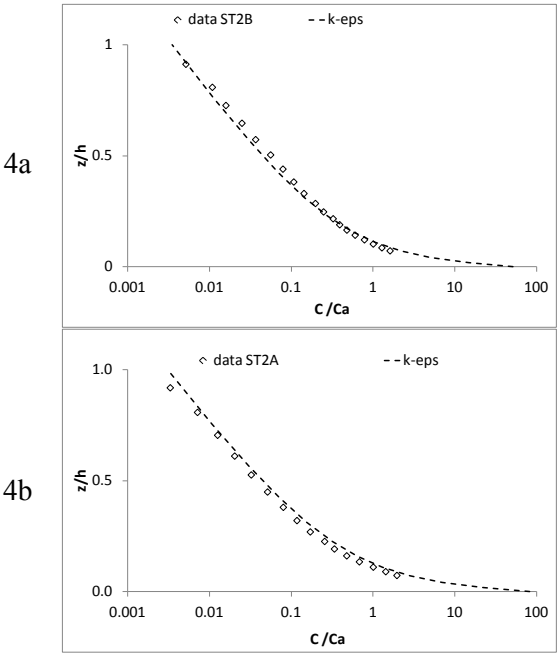

Figure 4. Comparison of NML and k-□ models for runs ST2B and ST2A: (a) concentration profile for ST2B run and (b) concentration profile for ST2A run.

VII. CONCLUSIONS

From the analysis of the experiences of Lyn [4, 8], the recommended modelling strategy is to use the k-ε model because it allows to obtain simultaneously the correct velocity and concentration profiles for the whole range of concentration levels. The NML model is efficient for the clear water runs but it appears to be less effective to reproduce the velocity profile in presence of sediment in suspension, even when the turbulence model is implemented in combination with damping functions. The comparison between TELEMAC-3D results and measured profiles of suspended sediment needs to be extended to other flume series, for example the experimental setup of Graf and Cellino [18], and validated with in-situ measurements.

ACKNOWLEDGEMENT

The authors would like to thank Professor Lyn for access to his dataset.

REFERENCES

[1] Amoudry L.O. and Souza A., 2011. Impact of sediment-induced stratification and turbulence closures on sediment transport and morphological modelling. Continental Shelf Research, 31, 912-928.

[2] Lesser G.R., Roelvink J.A., van Kester J.A.T.M and Stelling G.S. (2004) Development and validation of a three-dimensional morphological model. Coastal Engineering, 51 883-915.

[3] Tassi P., Villaret C., Huybrechts N., Hervouet J.M. : Numerical modelling of 2D and 3D suspended sediment transport in Tubulent Flows, RCEM 2011.

[4] Lyn D.A. (1991) Resistance in flat-bed sediment-laden flows. Journal of Hydraulic Engineering, vol. 117 (1).

[5] Villaret, C. and Davies, A.G. (1995) Modeling sediment turbulent flow interactions, Applied Mechanics Review, Vol.48, N°9, ASME, pp.601-609.

[6] Villaret C. and Trowbridge J.H. (1991) Effects of stratification by suspended sediments on turbulent shear flows, Journal of Geophysical Research, 96, C6, 10659-10680, 1991

[7] Rodi, W. (1993) Turbulence Models and Their Applications in Hydraulics, 3rd ed., IAHR Monograph, Rotterdam, The Netherlands.

[8] Lyn D. A. (1986) Turbulence and turbulent transport in sediment-laden open channel flows. Ph. D thesis, California Institute of Technology, Pasadena, California

[9] Nezu, I. and Nakagawa, H. (1993) Turbulence in Open-Channel Flows, IAHR Monograph, Rotterdam, The Netherlands.

[10] Munk, W.H. & E.A. Anderson (1948). "Notes on a theory of the thermocline", J. Marine Research, 3(1):276-295.

[11] Kranenburg C. (1998). Saturation concentrations of suspended fine sediment. Computations with the Prandtl mixing-length model. Report No.5-98, Faculty of Civil Engineering and Geosciences, Delft University of Technology.

[12] Graf W.H. and Cellino M. (2002) Suspension flows in open channels; experimental study. Journal of Hydraulic Research, vol. 40 (4).

[13] van Rijn, L.V (2003) "Principes of sediment transport in Rivers, Estuaries, Coastal Seas and Ocean", Lecture Notes Vol 1, University of Utrech, 327 p.

[14] Violeau, D., S. Bourban, C. Cheviet, M. Markofsky, O. Petersen, W. Roberts, J. Spearman, E. Toorman, H. Vested & H. Weilbeer (2000). Numerical simulation of cohesive sediment transport: intercomparison of several numerical models. Overview paper on COSINUS task E, 6th Int. Conf. On Nearshore and Estuarine Cohesive Sediment Transport (INTERCOH 2000), Delft, September 2000.

[15] Wilson, K.C (1989) Mobile-bed friction at high shear stress. Journal of Hydraulic Engineering, Vol. 115, (6), 825-830

[16] Sumer, B.M, Kozakiewicz, A, Fredsoe, J and Deigaard, R (1996) Velocity and concentration profiles in sheet-flow layer of movable bed. Journal of Hydraulic Engineering, Vol 122 (10), pp 549-558.

[17] Burchard H. (2002) Applied Turbulence Modelling in Marine Waters, 100, Lecture Notes in Earth Sciences. Springer Verlag, ISBN: 3-54043795-9.

[18] Cellino M. and Graf W. H. (1999) Sediment-laden flow in open-channels under noncapacity and capacity conditions. Journal of Hydraulic Engineering, Vol. 125 (5).